Symmetric Parsec-scale OH Megamaser Structures in Arp 220

COLIN J. LONSDALE
MIT Haystack Observatory,
Off Route 40
West ford, MA 01886;
cjl@wells.haystack.edu

PHILIP J. DIAMOND
National Radio Astronomy Observatory
Socorro, NM 87801
pdiamond@nrao.edu

HARDING E. SMITH[1]
Center for Astrophysics and Space Sciences
University of California, San Diego
La Jolla, CA 92093-0424;
hsmith@ucsd.edu

and

CAROL J. LONSDALE
Infrared Processing and Analysis Center
California Institute of Technology 100-22
Pasadena, CA 91125;
cjl@ipac.caltech.edu

Subject *headings:* galaxies: active — infrared: galaxies — radio lines: galaxies — masers

Received ____________________, accepted ____________________

---

[1] also, Infrared Processing and Analysis Center California Institute of Technology

ABSTRACT

The parsec-scale OH megamaser emission in the luminous IR galaxy Arp 220 has been imaged in detail using a global VLBI array. Four major emission regions are revealed in the 1667 MHz line, each with complex spatial and velocity structure showing intriguing symmetries. These emission regions have no associated continuum emission to stringent limits, and the brighter components have a maser amplification ratio exceeding 800. No compact emission is detected in the 1665 MHz line, demonstrating that at least two principal maser components are responsible for the emission in Arp 220, one diffuse and the other compact. The compact component, with high amplification and unmeasurable small 1665/ 1667 line rat io, appears to be the result of saturated masers in physically compact masing clouds. The diffuse component, on the other hand, appears to fit the traditional OH megamaser model of a low-gain ma-sing screen on scales of hundreds of parsecs. Infrared pumping is indicated for the diffuse component, but collisional pumping is probably important for the compact components. The compact components probably trace shock fronts in the dense nuclear environment, and may be related to AGN activity.

1. Introduction

OH rnegamasers are found in the nuclear regions of powerful infrared galaxies, and can have line luminosities approaching $10^4 L_\odot$. The prototype OH megamaser is found in the galaxy Arp 220 (IC 4553), and exhibits the classical properties of a double-peaked line profile a few hundred km/s wide, with a high ratio of 1667 MHz to 1665 MHz flux density (Baan, Wood and HaSchick, 1982, Henkel and Wilson 1990). The favoured interpretation of these masers has been that a low-gain masing screen distributed over a region a few hundred parsecs in size amplifies nuclear continuum emission from the galaxy. For Arp 220 such a model implies a covering factor of this screen of as low as a few percent, and an amplification factor of individual clouds within the screen as high as a few tens (Henkel and Wilson 1990, Randell et al., 1995).

Diamond et al. (1989) performed the first VLB1 observations of OH megamasers, showing that the OH structure in Arp220 was concentrated in two regions coinciding with the strong radio continuum emission. These data were consistent with the model mentioned above. The discovery that much of the OH luminosity originates in regions on scales of a few parsecs with amplification factors exceeding 50 (Lonsdale et al. 1994; LDSL94) modified this picture substantially, demonstrating that the masing gas is physically confined to a small volume, presumably deep in the twin nuclei of Arp 220. Many studies have indicated that the nuclear region of Arp 220 is heavily obscured by dust and gas, with some estimates of Av in excess of 1000 (Scoville, Yun and Bryant 1997). If these estimates are correct, radiation from the true nuclei can be observed directly only in the cm-submm bands, and in hard X-rays. The location and emission wavelength of compact nuclear OH megamasers therefore bestows new importance on their study as potentially powerful probes of the physical and kinematic conditions at the controversial central energy generation sites of ULIRGs.

The small physical extent of the masing clouds revealed by the LDSL94 data posed difficulties for conventional IR pumping schemes involving a cool (60K) extended (300pc) IR source, arguing instead for a smaller, warmer pump source. I, DSL94 favored a model involving a nuclear molecular torus surrounding a hidden AGN, simultaneously providing for a large OH mass in a small volume, and a plentiful local source of pump photons. In order to test this model, and to exploit the potential of the OH rnegarna.sers as probes of the IR galaxies, we conducted a major new VLBI imaging experiment on the four brightest OH rnegarnasers accessible to a northern VLBI array: Arp 220, II IZw35, IRAS F17208, and Mkn 231. All except Mkn 231 were imaged in OH. Here we present the main results of our spectral line imaging of Arp 220 at ~1 parsec resolution, deferring a detailed analysis of the extensive dataset to a future paper. The results for II IZw35 and IRAS F17208 are discussed by Diamond *et* al. (1997) and the continuum data for Mkn 231 are described in Lonsdale et al. (1997). In section 2 the observations and data reduction are described, and the results are presented. Section 3 deals with the implications of our results for the nature of OH megamasers and IR galaxy nuclei, A companion paper, Smith *et al.* (1997, SLLD97), presents the results of the continuum imaging for Arp 220.

2. Observations and Results

The observations, conducted under project code GL15 on 13 November 1994, involved 17 telescopes in Europe and the U. S., and covered three of the four OH maser lines plus the continuum. Arp 220 received a continuous 7-hour track, of which 4.2 hours was spent on-source, yielding excellent u-v coverage. The data were correlated on the NRAO VLBA correlator in Socorro NM in April 1996, with a spectral resolution of 15.1625 KHz (2.86 km/s).

The data were analyzed in January 1997 at the NRAO AOC in Socorro NM, using the 15 APR97 release of the AIPS package. Amplitude calibration was performed using telescope Tsys logs, while phasecal and delay determination was done using data on the calibrators 1300+580 and OQ208, which were observed periodically during the Arp 220 run. Complex bandpass calibrations were derived from data on 3C84 nearby in time. The fringe rates for Arp 220 were determined by fringe fitting to the line peak, which was clearly visible in the raw data on all baseline lengths. The antenna-based phases were corrected, and the amplitude calibration was refined, using self-calibration at the line peak. All these solutions, for phasecal, delay, rate, bandpass, phase and amplitude, were transferred uniformly to the rest of the line and continuum datasets.

The data were edited for discrepant points, and imaged using the AIPS IMAGR program. The angular resolution of the images was approximately 3.1 x 8.0 milliarcsec in (1.0 x 2.5 parsecs for Arp 220 at 76 Mpc). The rms noise level on the images was 1.3 mJy/beam at a spectral resolution of 2.86 km/s (15.625 KHz), and 0.03 mJy/beam in the continuum images with 26 MHz bandwidth. Images were made at a variety of spectral resolutions, both with and without tapering in the uv plane, in order to provide optimum sensitivity to features of diverse properties. We have chosen a small subset of these images for display here, in order to best illustrate the principal results of the study. Figures 1 and 2 show the morphology of the compact OH emission in the western and eastern nuclei respectively, along with component spectra, and velocity profiles across the brightest feat ures. The images presented by Diamond et al. (1989) are broadly consistent with the much higher quality data presented here. The continuum images, which show numerous sub-mJy unresolved point sources interpreted as highly luminous starburst-related radio supernovae, are presented and discussed in the companion paper by Smith *et al.* (1997, SLLD97), and are not shown here, though we frequently refer to these results.

2.1. Maser **Emission Characteristics**

Arp 220 has two nuclei in the radio and near-infrared continuum, separated by about 0.95″(Condon et al. 1991, Mozzarella et al. 1992). There are four major regions of OH maser emission, two in the western nucleus and two in the eastern nucleus. In each nucleus, one of the emission regions has a highly elongated structure, and one has a more amorphous structure with generally slightly less compact features. The velocity ranges of the four components overlap each other significantly. In each nucleus the more redshifted, linear component is to the north, and the more blueshifted, amorphous component is to the south. We adopt labels W 1, W2, El and E2 for the four components, where the first character refers to the nucleus in which the component resides, "1" refers to the linear, redshifted northern component, and "2" refers to the amorphous, blueshifted southern component.

Component WI shows a narrow, linear ridge of emission about 25 pc long and less than lpc wide oriented in position angle ~ 150 degrees, with a compact central feature spanning many velocity channels that is spatially unresolved in individual velocity channels. This central feature displays evidence of a marginal] y resolved, nonlinear transverse velocity gradient. The linear ridge displays a well defined, symmetric velocity gradient of ~3 km/s/pc, with increasing blueshift away from the central feature on both sides (i.e. the ends of the structure are blueshifted, and the center is redshifted). There is no significant curvature in the overall structure of W1, which with the exception of the bright central feature, has a smooth appearance at this resolution.

Component W2 consists of a slightly resolved ridge oriented roughly N-S, with a more diffuse region of emission immediately to the east. The velocity structure is complex. The overall extent of the main component is roughly 15x 10 pc. About 15 pc to the SW is a barely resolved maser feature $\leq$ 2pc across which is blueshifted from the main W2 component by ~100 km/s. The W2 component is spectrally very broad, and is located near the southern edge of a cluster of continuum point sources (SLLD97), none of which are coincident with the strong maser features.

In the eastern nucleus, component El consists of a string of compact maser spots about 30pc long oriented roughly EW, which curves smoothly through about 30 degrees along its length. Most of the maser spots have relatively narrow velocity width, of order 20-40 km/s. One component, however, located at the center of the string of spots, has a very broad velocity width of more than 150 km/s. This component, and to a lesser extent all those to its west (but not those to the east) display a sharp velocity gradient approximately perpendicular to the overall elongation of El. The individual maser spots are generally barely resolved (source sizes 1 to 2 PC).

Component E2 is morphologically similar to component W2, with a narrow, barely resolved ridge of emission $\sim$ 10pc long, and more diffuse emission to the west of the ridge. The velocity structure is complex, with an overall SE to NW gradient superimposed.

The central features of components W1 and El stand out among the compact maser spots in terms of their brightness and broad velocity width. The fact that each of these unusual maser spots accurately bisects the angular extent of the elongated structures containing them constitutes a symmetry property of components W 1 and El that requires explanation.

There is *no evidence of compact continuum* emission *above a level of 0.1 mJy* coincident with any of the four major emission regions.

In addition to the four main maser components, several weak isolated maser spots are seen, generally confined to the vicinity of one or the other nucleus. These spots are compact and spectrally narrow. Two weak ($\sim$ 5mJy), unresolved maser components, position ally coincident with each other but separated by 160 km/see in velocity, are detected which are aligned with one of the continuum sources (source NW 10 of SLLD97) to $\sim$1 mas.

We are able to account for roughly two thirds of the total 1667 MHz line luminosity of Arp 220 between 5250 and 5500 km/s, leaving roughly one third to be accounted for by the diffuse maser component. Due to limited sensitivity, particularly to multiple weak compact sources, the contribution of compact emission to the line wings is less well determined.

We also imaged the source in the 1665 MHz line, anticipating emission at about 20 percent of the strength of the 1667 MHz emission, in accord with the line ratio from single-dish measurements. Instead, the 1665 MHz emission is conspicuously absent to stringent levels across the entire field of view. For the brightest maser features, the 1667/1665 line ratio exceeds 100, and for all features has only a lower limit. We conclude that all the 1665 MHz emission is diffuse, and that the diffuse OH maser emission on scales of 0.1 arcsec and greater has an approximately thermal line ratio of 1.6 corresponding to the low-gain limit. We also failed to detect compact 1720 MHz emission from Arp 220, suggesting that this line also arises in the diffuse maser gas.

'I'he lack of positional coincidence between the continuum sources and maser features demonstrates that, ignoring the possibility of variability, the alignment of line and continuum interferornetric phases reported by LDSL94 was a chance coincidence. The maser amplification factor calculated in that paper under the assumption of complete line/continuum overlap was therefore conservative. A lower limit to the amplification factor for the brightest spots, based on direct measurement, is $\sim$800.

3. **Discussion**

3.1. **The Diffuse Maser Component**

Hitherto, the overall properties of OH megarnasers have been interpreted in terms of a single maser component, with a particular cloud gain and covering factor (Henkel and Wilson 1990, Randell et al. 1995). The results presented here instead show that the OH masers in Arp 220 are of at least two main types, one diffuse and the other compact, with sharply distinct observational characteristics. We have shown that the diffuse component shows low amplification ($\leq$ 1) in Arp 220, with an approximately thermal 1667/1665 line ratio. This emission is well explained by a conventional OH megamaser model with relatively low cloud gain, relatively high cloud covering factor, and pumping from the far-IR radiation field. It is this component which is almost certainly related to the OH absorption lines in the mid-IR recently detected by 1S0 (Skinner et al. 1997).

The precise alignment of two maser spots with the continuum source NW 10 (SLLD97) unambiguously indicates unsaturated maser emission in foreground clouds, while the large velocity difference between the two spots suggests a substantial physical separation of the clouds from each other, and probably from the continuum source. These properties indicate that the masing gas responsible is associated with the diffuse maser component. The measured gains of $\sim$ 5 for these spots, if typical of all clouds in the diffuse maser, would imply a covering factor of $\sim$ 0.06, and a 1667/1665 line ratio somewhat larger than is implied by our data. The gain of the diffuse maser is therefore probably a function of position, and is locally higher in the vicinity of these maser spots.

3.2. The Compact Maser Component

The compact maser component is characterized by high gain, very high 1667/1665 line ratio, high brightness temperature, and a filamentary appearance with very high axial ratios.

The observational lower limits on the maser amplification factors range up to 800, set by the limit on positionally coincident continuum emission. For one of the main maser spots, W 1, we can infer that the amplification is likely to be significantly higher even than this limit. 'l'here is no evidence for compact continuum emission in Arp 220 other than the isolated unresolved components we interpret as radio supernovae (SLLD97), and we assume that additional compact continuum components below our detection threshold have a similar character. The structure of maser component W 1, of which the compact central peak is clearly an integral part, is qualitatively different from that of the compact continuum, leaving the diffuse continuum as the only background radiation available for amplification. The peak of component W1 has an upper size limit of $\sim 0.1 \mathrm{pc}^2$, corresponding to at most $\sim 4\mu\mathrm{Jy}$ of diffuse continuum flux behind the masing cloud available for amplification. Since we see over 70 mJy of line flux from this feature, an amplification factor well in excess of 10^4 is implied. Since WI lies $\sim 0.25''$ north of the diffuse continuum emission from the NW nucleus (e.g. Baan and Haschick 1995), even this figure is likely to be an underestimate.

Saturation of the compact masers is suggested by the general absence of evidence for amplification of background continuum emission, in conjunction with the high deduced gains and measured brightness temperatures of up to 10^{10}K. This conclusion differs from that of LDSL94 who were able to mea-sure only a relatively modest lower limit on the amplification factor.

The observed sizes of the compact masing spots probably correspond closely to the true projected physical sizes of the masing clouds. Most of the individual maser spots in Arp 220 are compact, measuring less than a few parsecs, yet they generally display linewidths of several tens of km/s, compared to natural linewidths of much less than 1 km/s. This sharply reduces the likelihood that the maser spots sample a large ma-sing cloud along a particular velocity-coherent line of sight. We note that the broad velocity widths of individual maser spots contributes significantly to the breadth of the integrated OH spectrum of Arp 220, contrary to previous assumptions that large-scale rotational motions in an ensemble of clouds was responsible (e.g. Staveley-Smith *et al.* 1992).

We now address the question of the pumping mechanism for the compact masers. First we note that any model for the pumping mechanism must satisfy the constraint that maser radiation occurs into a large fraction of 4π steradians. This follows from the observed ubiquity of OH rnegamasers among powerful IR galaxies (Sanders et al. 1988, Baan 1989), implying a total luminosity of the Arp 220 OH megamasers of order 5001,..

Given the small physical extent of the ma-sing regions, far-infrared pumping mechanisms are strongly constrained due to geometrical considerations, as noted by I, DSL94. Using a simple model of a spherical maser of radius r_m embedded in a uniform spherical IR pump source of radius r_p, the solid angle Ω_m of the maser subtended from the pump, and therefore the fraction of the IR luminosity available for pumping, is

$$\Omega_m = 2\pi \left[1 - \frac{(r_p^2 - r_m^2)^{3/2}}{r_p^3} + \frac{r_m^3}{r_p^3} \right]$$

For $r_p/r_m \sim$ 30, appropriate for Arp 220 based on our data, this gives $\Omega_m =$ 1.7 x 10-3, While this value depends significantly on maser geometry, and the pump requirements depend on poorly determined maser beaming angles, it is clear that the small measured maser sizes require large increases in estimated I R pump efficiencies. Requirements are likely to be more severe for intense, compact masers far from the radio continuum sources which are thought to coincide with the far-l R sources. Generally, IR pump photon efficiencies are thought to be below 1 ‘%0 (Randell et al. 1995). For Arp 220, simple application of the above solid angle results in a pump photon efficiency greater than unity, calling into serious question the viability of infrared pumping of compact OH megamasers.

We see two ways of alleviating this constraint on infrared pumping models. First, the compact masers could lie in thin sheets which subtend large solid angles from the IR source, and thus intercept the bulk of the IR photons. Long gain paths are possible only in the plane of a sheet, naturally explaining the filamentary appearance of components W 1 and El, but not the more amorphous appearance of W2 and E2. Portions of the sheets which do not participate in long gain paths could account for the diffuse maser component. A problem is that the transverse compactness of the observed masers places extreme requirements on the sheet size to thickness ratio, the physical basis for which is not apparent. Also, this model does not naturally account for the symmetry properties of W 1 and El.

Second, following the suggestion of LDSL94, each compact maser component may have its own small, local IR source, from which the masing gas subtends a large solid angle. We note, however, that the minimum blackbody size for a 60K IR source of sufficient photon flux to pump these masers is on the order of 100Pc, implying that the hypothesized local IR pump sources are much warmer than 60K. LSDL94 proposed that the pump source could be a mid-infrared luminous molecular torus surrounding an AGN. This model now seems unreasonable because there are two major maser components in each nucleus, not one, and in addition, the kinematics of each maser component are inconsistent with a simple torus model. The nature of any hypothetical compact local IR pump source is therefore unclear.

Given these problems with infrared pumping, we consider the possibility that the pump could be collisional. The filamentary appearance of W 1 and El suggests shock fronts, which would heat and compress a molecular medium estimated to have an ambient density exceeding $10^4 \mathrm{cm}^{-3}$ (Scoville, Yun and Bryant, 1997), sharply enhancing collision rates with H_2 and perhaps giving rise to the masers. Gray (private communication) suggests that collisional pumping is possible in regions of $n_H \approx 10^6 \rightarrow 10^7$ and with IR sources of temperature 25K to 50K, the IR source essentially provides a catalyst for the pump action to begin.

One possible source of shock waves is the supernovae associated with the starburst. Most of the mechanical energy input and consequent shocks would be expected to be close to the continuum radio sources, identified as recent radio supernovae (SLLD97), true for three of the four compact maser components. However, the coherence of the maser structures on 20-30pc scales indicates large-scale disturbances associated with each starbursting region as a whole as a more likely source of shocks than small scale disturbances associated with individual supernovae. The observed systematic velocity gradients in components W1 and El may indicate shear across a shock front, possibly associated with the generation of the large scale superwind observed in Arp 220 (Heckman *et* al. , 1996). Nevertheless, there is no ready explanation in this picture for the morphological differences between components 1 and 2 in each nucleus, nor for the central feature symmetry which is prominent in both W1 and El.

Another possibility is that the bright, spectrally broad feature in the middle of both W1 and El could arise from collisionally pumped OH in a molecular torus orbiting the central mass of two newly formed AGN nuclei. This possibility is supported by a clear transverse velocity gradient in El (fig 2(b)), and indications of such a gradient in W 1 (fig 1(c)), The mean gradients are of order 50 km/s/pc, corresponding to an enclosed mass density of $\sim 7 \times 10^7 M_\odot \mathrm{pc}^{-3}$, and a total enclosed mass of order $10^8 M_\odot$. One might expect the central engines to be well fed in such an environment, and the Eddington luminosities for two black holes of this mass exceed the total bolometric luminosity of Arp 220 by a factor of a few, implying that such putative AGNs could be energetically important. The strikingly symmetrical, elongated features on either side of the central feature might be regions shocked by the passage of twin AGN jets, and the curvature apparent in El could be analogous to the curvature in head-tail radio sources caused by lateral ram pressure due to motion through the ambient medium. The lack of such curvature in W1 may be due to the plane of curvature falling in the line of sight, a conjecture supported by the striking velocity signature of this component. Curvature in a plane containing the line of sight, coupled with some acceleration of the shocked material by the jets would produce the observed velocity structure. This model does not account for components W2 and E2, and we speculate that higher sensitivity observations might reveal physical connections to the putative AGN nuclei if this hypothesis is correct. Large optical depths to the locations of the AGN sources at mid-infrared wavelengths could account for the absence of AGN-related high-excitation lines (Sturm et al. 1996).

We conclude that the OH megamasers in Arp 220 have two distinct types, one diffuse and the other compact. The diffuse masers are unsaturated, of low gain, and are pumped by IR radiation. The compact masers appear to be saturated, collisionally pumped, and probably trace shock fronts in the dense nuclear molecular medium. It is interesting that some OH megamasers have high 1667/1665 MHz line ratios, and display high OH to FIR luminosity ratios, exacerbating IR pumping requirements (Staveley-Smith *et al.* 1992). We speculate that these systems are dominated by collision ally pumped compact maser components similar to those described here. Much of the broad megamaser linewidth is intrinsic to the compact maser spots, and is not due to large-scale rotational motions of an ensemble of clouds. The properties of the compact masers in Arp 220 suggest that they may trace newly formed AGN molecular tori and jets. Future higher sensitivity observations should clarify this issue.

CJL and HES thank the NRAO AOC for hospitality and assistance. HES wishes to express gratitude to IPAC for providing continued support. IPAC/JPL is supported by NASA. Haystack is supported by the NSF via NEROC. The National Radio Astronomy Observatory is a facility of the National Science Foundation operated under cooperative agreement by Associated Universities, Inc. Support of this project at UCSD has been provided by the NSF under grant AST93-19895.

REFERENCES

Baan, W.A. 1989, ApJ, 338, 804.

Baan, W.A. & Haschick, A.D. 1995, ApJ, 454, 745.

Baan, W. A., Wood, P.A.D. & Haschick, A.D. 1982, ApJ, 260, 1.49.

Condon, J. J., Huang, Z.-P., Yin, Q. F., & Thuan, T.X. 1991, ApJ, 378, 65.

Diamond, P. J., Norris, R. P., Baan, W. A., & Booth, R.S. 1989, ApJ, 340, 1,49.

Diamond, P. J., Lonsdale, C. J., Smith, H. E., & Lonsdale, C.J. 1997, *submitted to* ApJ.

Heckman, T. M., Dahlem, M., Eales, S. A.; Fabbiano, G. & Weaver, K. 1996, ApJ, 457, 616.

Henkel, C. & Wilson, T. I,. 1990, A&A, 229, 431.

Lonsdale, C. J., Diamond, P. J., Smith, H.E. & Lonsdale, C.J. 1994, *Nature*, 370, 117 (LDSL94).

Lonsdale, C. J., Lonsdale, C. J., Diamond, P.J. and Smith, H.E. 1997, in preparation.

Mozzarella, J. M., Soifer, B. T., Graham, J. R., Hafer, C. I., Neugebauer, G. & Matthews, K. 1992, AJ, 103, 413.

Randell, J., Field, D., Jones, K. N., Yates, J.A. & Gray, M.D. 1995, A&A, 300, 659.

Sanders, D. B., Soifer, B. T., Elias, J. H., Madore, B. F., Matthews, K., Neugebauer, G. & Scoville, N.Z. 1988, ApJ, 325, 74.

Scoville, N. Z., Yun, M. & Bryant, P. 1997, ApJ, in *press*.

Skinner, C. J., Smith, H. A., Sturm, E., Barlow, M. J., Cohen, R.J. & Stacey, G.J. 1997, *Nature, 386, 472.*

Smith H. E., Lonsdale, C. J., Lonsdale, C.J. & Diamond, P.J. *1997, submitted to* ApJ (SLLD97).

Staveley-Smith, L., Norris, R. P., Chapman, J. M., Allen, D. A., Whiteoak, J.B. & Roy, A.L. MNRAS, 258, 725.

Sturm, E., Lutz, D., Genzel, R., Sternburg, A., Egami, E., Kunze, D., Rigopoulou, D., Bauer, O. H., Feuchtgruber, H., Moorwood, A.F.M. & De Graauw, T. 1996, A&A, 315, 1,133.

Fig. 1.— The western nucleus of Arp 220. The angular resolution in Fig. l(a) is 3,1 x 8.0 milliarcsec (1.1 x 2.9pc) in p.s. $\sim$ 0°, but Fig. l(b) has been tapered to a resolution of 8 x 8 milliarcsec (2.9 x 2.9pc) due to poor snr in the full-resolution image. More compact structures than this are present in component

This manuscript was prepared with the AAS LaTeX macros v4.0.

W2. Contour levels are separated by a factor of 2*. Fig. l(a) is averaged over the velocity range 5300-5400 km/s, while Fig. l(b) is averaged over the velocity range 5200-5450 km/s. Fig l(c) shows the transverse velocity profile across the peak of WI, while Figs. l(d) and l(e) show the integrated spectra of W1 and W2 respectively.

Fig. 2.— The eastern nucleus of Arp 220. Fig. 2(a) shows the image of the eastern nucleus of Arp 220 in the 1667 MHz OH line. The angular resolution and contour levels are the same as those in Fig l(a), and the emission has been averaged over the velocity range 5300-5500 km/s. Fig 2(b) illustrates the transverse velocity gradient across the bright central feature of component El. Figs. 2(c) and 2(d) show the integrated 1667 MHz spectra of components El and E2 respectively.

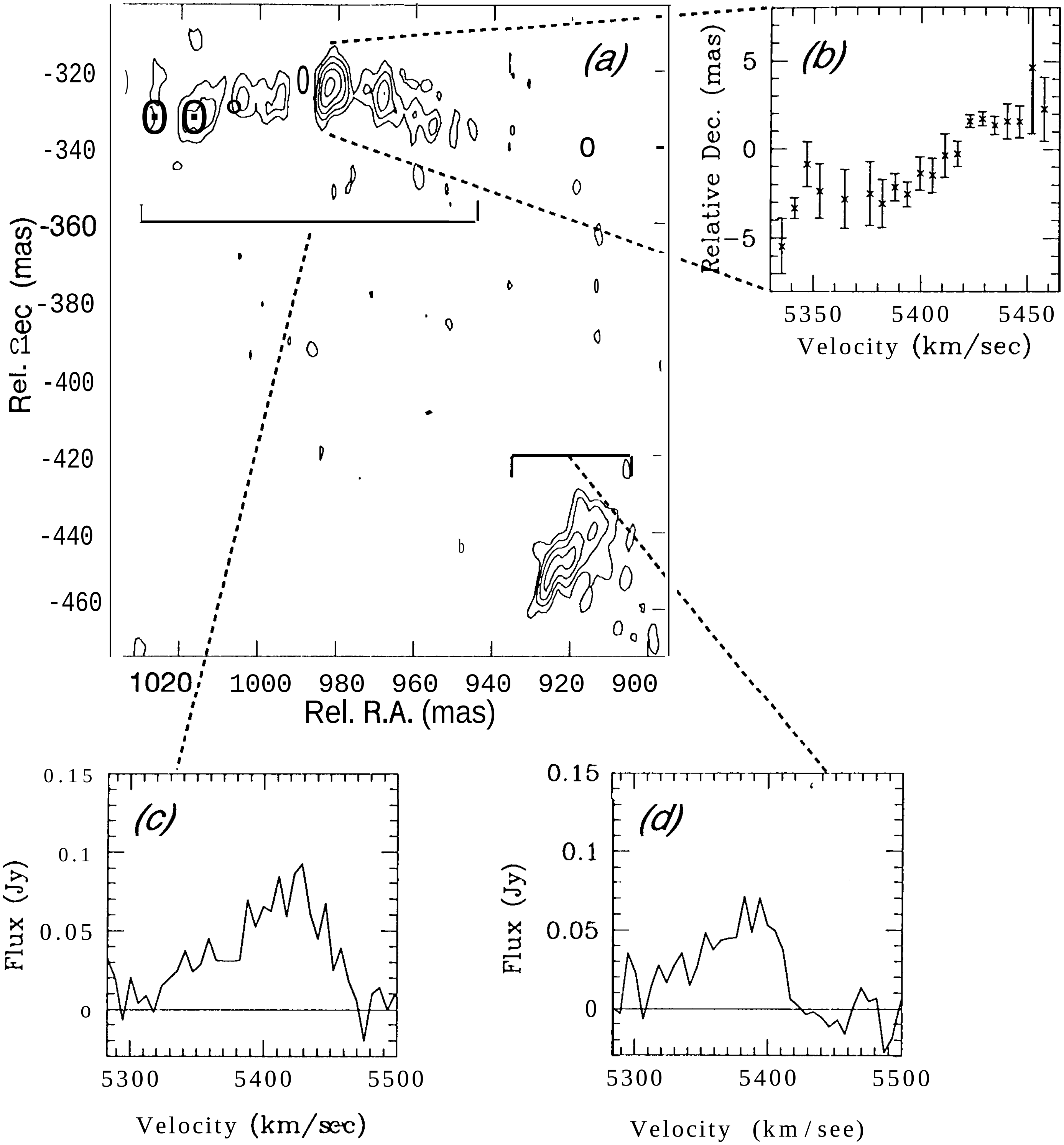
(a)
-320
-340
-360
-380
-400
-420
-440
-460
Rel. Dec (mas)
1020
1000
980
960
940
920
900
Rel. R.A. (mas)
(b)
5
0
−5
Relative Dec. (mas)
5350
5400
5450
Velocity (km/sec)
(c)
0.15
0.1
0.05
0
Flux (Jy)
5300
5400
5500
Velocity (km/sec)
(d)
0.15
0.1
0.05
0
Flux (Jy)
5300
5400
5500
Velocity (km/see)

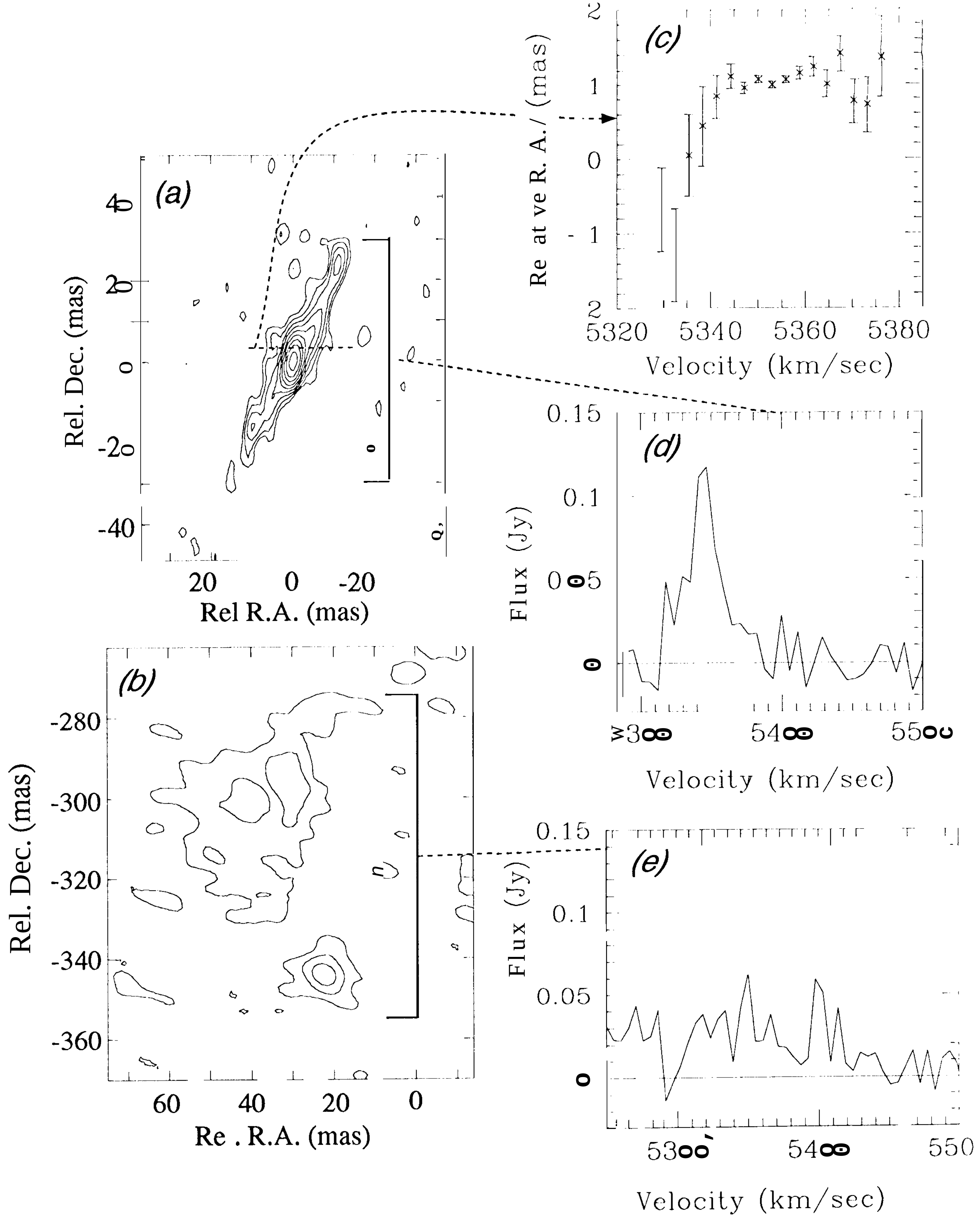

(a)
Rel. Dec. (mas)
Rel R.A. (mas)
(b)
Rel. Dec. (mas)
Re . R.A. (mas)
(c)
Re at ve R. A./ (mas)
Velocity (km/sec)
(d)
Flux (Jy)
Velocity (km/sec)
(e)
Flux (Jy)
Velocity (km/sec)